



Modification of hyperbranched hemicellulose polymer and its application in adsorbing acid dyes

Linya Zhang · Wei Xue · Limin Gu

Received: 20 February 2019 / Accepted: 6 May 2019 / Published online: 11 May 2019
© Springer Nature B.V. 2019

Abstract The paper presented a new, non-pollution macromolecule of adsorbing acid dyes, and developed the adsorption mechanism on the basis of effect between the modified groups of hyperbranched hemicellulose polymer and acid dyes. The modified hyperbranched hemicellulose polymer (HHP) with a large number of terminal carboxyl groups and hydroxyl groups was synthesized by hemicellulose maleate and dihydroxymethyl propionic acid. The degree of substitution, kinematic viscosity and thermal stability of HHP was determined. In SEM images, the HHP exhibited the pores and cross-linked structure which were good help for dye adsorption. When the HHP was applied in adsorbing Methyl red dye, Bromocresol green dye and Bromophenol blue dye, it exhibited higher adsorption capacity. The adsorption capacity changed with different adsorbent dosage, pH, temperature and ionic strength, and the optimal

adsorption capacity for Methyl red dye, Bromocresol green dye and Bromophenol blue dye could reach 825 mg/g, 675 mg/g and 912 mg/g respectively. The adsorption mechanism, adsorption isotherm and adsorption diffusion mode were demonstrated by Pseudo-order model, Langmuir model, Intraparticle diffusion model and Memberance diffusion model respectively. The adsorption data possessed better correlation with Pseudo-second-order model, Langmuir model and Intraparticle diffusion model. The adsorption isotherms and thermodynamic data indicated the processes of HPP2 adsorbing three acid dyes were endothermic. The N_2 -adsorption/desorption isotherms of HPP2 revealed the hyperbranched hemicellulose polymer filled the pore in clusters, and its adsorption process met with monolayer adsorption.

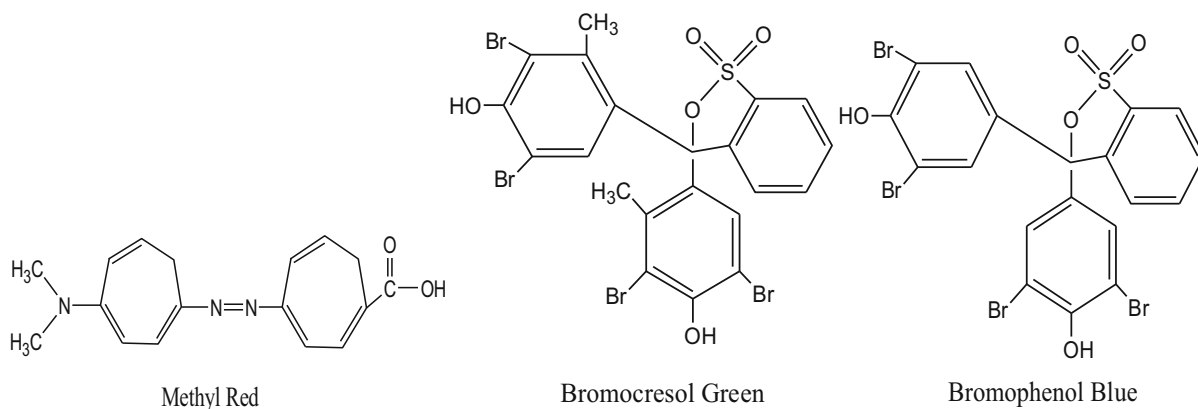
L. Zhang (✉) · W. Xue · L. Gu
College of Chemical and Pharmaceutical Engineering,
Hebei University of Science and Technology, No. 26
Yuxiang Street, Shijiazhuang 050018, Hebei, People's
Republic of China
e-mail: ly10805010@163.com

Some scientists have noticed hemicellulose, a renewable natural macromolecule, which was abundant in plants accounting for about one-third of plant resources. Hemicellulose contained a lot of hydroxyl groups which could be modified by the method of hyperbranching and introducing the different active groups to gain some appropriate characteristics such as hydrophobicity, thermoplasticity, water solubility, surface activity and biological functionality (Esposito and Antonietti 2015; Lu et al. 2015). Ferrari studied the hemicellulose modified by polyacrylic acid to gain the hydrogels. The hydrogels had strong hydrophilicity and swelling ability, and showed remarkable adsorption ability for Cu^{2+} , Cd^{2+} , Pb^{2+} , Zn^{2+} , Ni^{2+} and Co^{2+} (Ferrari et al. 2015). Rahman had modified the hemicellulose with methyl methacrylate. The modified hemicellulose adsorbent had super adsorption effect on Cu^{2+} , and the adsorption capacity reached to 305.3 mg/g (Rahman et al. 2017). Due to the favorable biocompatibility (Tirtom et al. 2012; Tripathi et al. 2016; Wang et al. 2013), the modified hemicellulose had drawn extraordinary attention in field of adsorbing organic dyes (Guijarro-Aldaco et al. 2011).

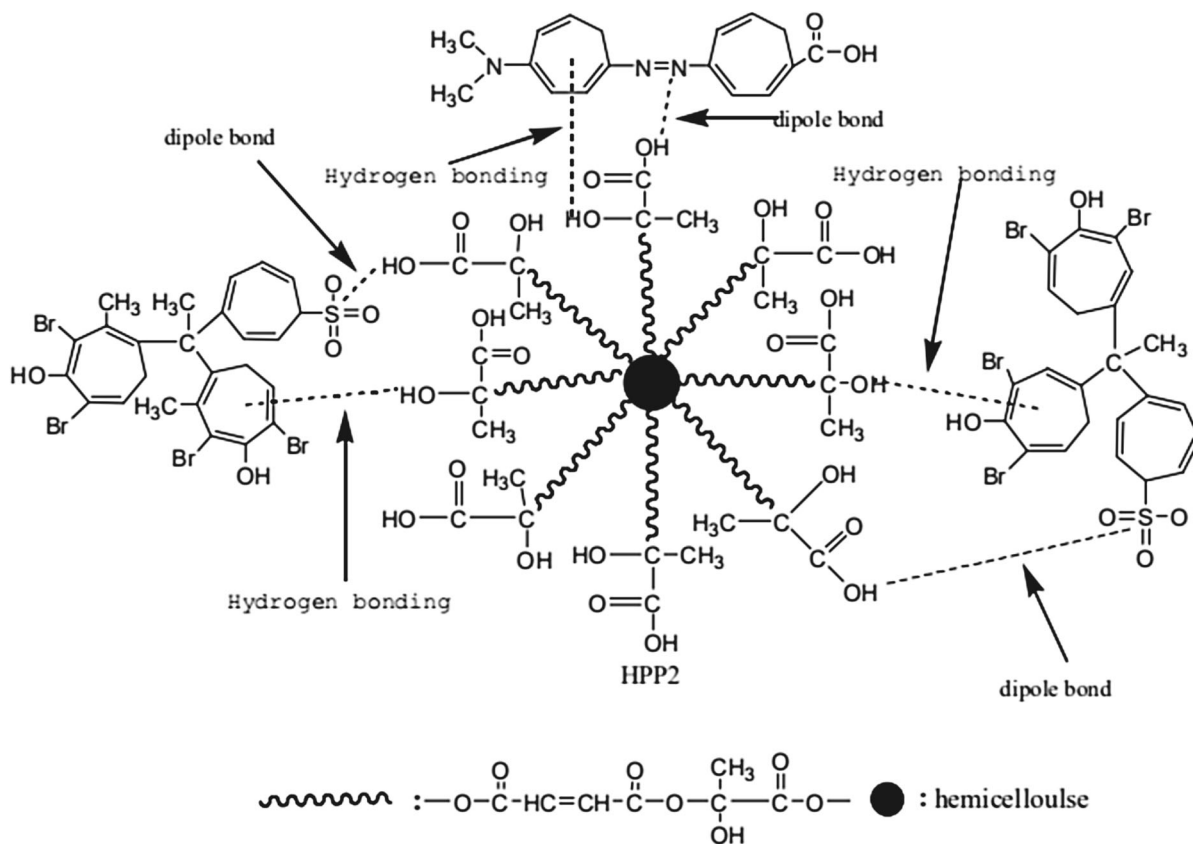
Hyperbranched polymer was a kind of macromolecule with high branching structure and a large number of active end groups, which could be synthesized and modified easy by one step reaction (Sun et al. 2017; Li et al. 2012; Ragauskas 2006). The hyperbranched polymer could take on some advantages such as simple design, easy operation, low cost and wide suitability. Some researchers had reported the hyperbranched polymers in adsorbing dyes (Luo et al. 2010; Kanekiyo et al. 2008). For example, Liu and his colleagues studied the

hyperbranched polymeric ionic liquid with imidazolium backbones, and it was used to remove the anionic dyes from water (Schutyser et al. 2018). Delidovich and his group reported that the hyperbranched polymer could express the excellent selectivity, and they prepared the multi-responsive microgel to adsorb the hydrophilic dyes (Ning et al. 2016).

Based on the above characteristics of hemicellulose and hyperbranched polymer, our efforts focused on integrating the advantages of two polymers to be suitable as a new, non-pollution acid dyes absorbent. In our study, the modified hyperbranched hemicellulose polymer HPP1 and HPP2 with terminal carboxyl groups and hydroxyl groups were synthesized by hemicellulose maleate and dihydroxymethyl propionic acid step by step. The acid dyes such as Methyl red dye, Bromocresol green dye and Bromophenol blue dye with anionic groups were chose to study the adsorption process of the modified hyperbranched hemicellulose polymer (Scheme 1). The adsorption between the modified hyperbranched hemicellulose polymer and acid dye depended mainly on dipole bonding and H bonding forces. The carboxyl group of the modified hyperbranched hemicellulose polymer and the sulfonate or azo group of acid dye formed the dipole bonding, while the hydroxyl of the modified hyperbranched hemicellulose polymer and hydroxyl or benzene of acid dye formed the H bonding (Scheme 2). The adsorption capacity of the modified hyperbranched hemicellulose polymer was discussed by the dosage, pH, temperature and ionic strength. Moreover, the adsorption mechanism, adsorption isotherm and adsorption diffusion mode were evaluated by Pseudo-order model, Langmuir



Scheme 1 The structure of methyl red dye, bromocresol green dye and bromophenol blue dye



Scheme 2 The modified hyperbranched hemicellulose polymer adsorbed methyl red dye, bromocresol green dye and bromophenol blue dye

model, Intraparticle diffusion model and Membrane diffusion model.

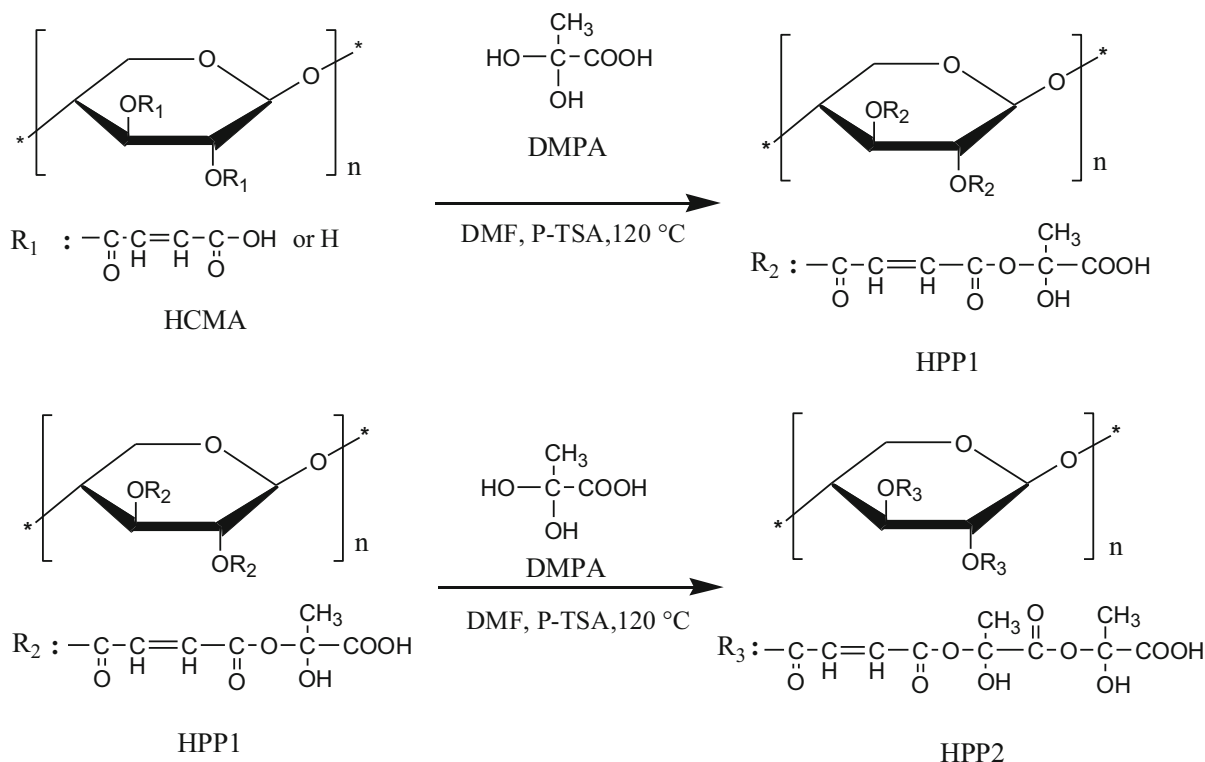
Hyperbranched hemicellulose polymer possess a large number of active end groups, and it can be easily prepared. The different end groups can take the adsorption targeted and the absorbent dose reduced. Also, the hyperbranched hemicellulose polymer can be easily degraded. These advantages indicate that hyperbranched hemicellulose polymer can be applied better as an ideal dye absorbent.

Experimental

Material

Hemicellulose maleate (HCMA, Molecular weight 24,372, DS 0.97) was synthesized from hemicellulose

and Maleic anhydride. Hemicellulose (Xylose 80.63%, mannose 11.16%, glucose 6.26%, galactose 1.22%, glucuronic acid < 0.72%, Molecular weight 11,665–14,268) was obtained from Sanyou co. (Tangshan, China). Maleic anhydride (AR), N,N-Dimethylformamide (DMF, AR), sodium hydroxide (NaOH, AR), P-toluenesulfonic acid (P-TSA, AR) and Sulfuric acid (H₂SO₄, AR) were purchased from Xiandai reagent Co. (Shijiazhang, China). 2,2-Bis(hydroxymethyl)propionic acid (DMPA, AR) was purchased from Aladdin Co. (Shanghai, China). Methyl red dye (AR), Bromocresol green dye (AR) and Bromophenol blue dye (AR) were purchased from yongfa Co. (Tianjin, China).



Scheme 3 Synthesis of the modified hyperbranched hemicellulose polymer

Synthesis of the modified hyperbranched hemicellulose polymer

Hyperbranched hemicellulose polymer HHP1 was synthesized from HCMA and DMPA (Scheme 3). Typically, HCMA (2.4 g), DMPA (3.88 g), P-TSA (0.25 g) and DMF (35 mL) were mixed in a flask. The mixture was stirred at 120 °C under nitrogen atmosphere. The reaction was ended at a constant acid value. After reaction, the resulted HHP1 was thoroughly washed with 95% ethanol, and then dried in a vacuum oven at 40 °C for 24 h.

The modified hyperbranched hemicellulose polymer HHP2 was synthesized from HHP1 (3.3 g), DMPA (7.88 g) and P-TSA (0.45 g) on the same synthetic route as HHP1.

IR (KBr): 3450 cm^{-1} (–OH), 2920 cm^{-1} (–CH₃), 1750 cm^{-1} (–COO–), 1720 cm^{-1} (–COOH), 1690 cm^{-1} (–C = C–).

¹³C-NMR (400 MHz, D₂O, δ): 178 ppm (CH₃–CHOH–COOH), 172 ppm (CH₃–CHOH–COO), 166 ppm (O = C–CH = CH–COOH), 135.6 ppm

(O = C–CH = CH–COO), 112.3 ppm (CH₃–CHOH–O), 102.4 ppm (O–CH₂–O), 85 ppm (–CH₂–O–CH₂–), 76 ppm (CH₃–CH₂–CH₂OH), 73.6 ppm (CH₃–CHOH–CH₂OH), 73.1 ppm (OHCH₂–CHOH–CH₃), 63.2 ppm (–CH₂–CH₂–O–CH₂–), 58 ppm (–CH–CH₃–O–), 23.3 ppm (–CH–COOH) and 22.3 ppm (CH₃–CHOH–COOH). The spectral peaks were signed as r, o, k, m, p, a, f, d, c, b, e, g, h and q separately in the molecular formula (Fig. 3a–c).

Measurements

In followed measurements, the data from all the experiments were built on measuring three times to get the accurate value.

The degree of substitution (DS) was measured by pH Meter to characterize the modified degree of sample. The HHP (0.1 g) was added in water (40 mL), and the pH was adjusted to 8.2 by adding NaOH (0.1 mol/L). Then adding H₂SO₄ (0.1 mol/L) to titrate it until the pH reached to 3.7. The DS was calculated from the following Equations (Moran et al. 2012):

$$DS = 0.168B/(1 - 0.08B) \quad (1)$$

$$B = 2 \text{ MV/m} \quad (2)$$

where the M represented molality of H_2SO_4 (0.1 mol/L), V represented the volume of H_2SO_4 consumed, m represented the weight of sample and B represented the content of Sodium acetate per gram of sample.

The kinematic viscosity was measured by kinematic viscosity tester SC-265B. The time t and t_0 of the sample (0.01 g/mL) and blank sample flowing through the capillary viscometer at room temperature were recorded respectively. The data of the kinematic viscosity were calculated from the following Equations (Bodnar et al. 2007):

$$\Gamma = 2 * (\Gamma_s - \ln \Gamma_r)^{1/2} / 2 \quad (3)$$

$$\Gamma_s = \Gamma_r - 1 \quad (4)$$

$$\Gamma_r = t/t_0 \quad (5)$$

where Γ was the kinematic viscosity, the time t (s) and t_0 (s) represented the time of sample (0.01 g/mL) and blank sample flowing through the capillary viscometer respectively.

Fourier transform infrared (FT-IR) spectra were taken on a Thermo Nicolet Nexus 670 spectrometer by scanning 20 times with a resolution of 4 cm^{-1} within a spectral range of $450\text{--}4000 \text{ cm}^{-1}$.

^{13}C -NMR spectra were obtained by a Bruker-400 MHz spectrometer using D_2O as solvent, and Me_4Si was used as internal standard at room temperature.

The morphology of the samples were studied with SEM S-4800-1. The samples were adhered to conductive adhesive and sprayed with gold before fractographic examination.

The thermal decomposition profiles of the samples were studied with TG/DTA6200 at a constant rate of $10 \text{ }^\circ\text{C}/\text{min}$ in nitrogen atmosphere from 30 to $600 \text{ }^\circ\text{C}$.

The N_2 -adsorption/desorption isotherms were obtained by Micromeritics TriStar volumetric adsorption analyzer 3020 at $-196 \text{ }^\circ\text{C}$. The amount adsorbed was measured with the change of relative pressure P/P_0 , where the P was the true pressure of N_2 and P_0 was the saturated vapor pressure at the measured temperature.

The adsorption capacity was measured by Ultraviolet spectro photo meter TU-1810. First, the standard curves of Methyl red dye, Bromocresol green dye and Bromophenol blue dye were obtained by measuring

the absorbance of standard solution at different initial concentration. Second, adding the sample (0.01 g) to Methyl red dye (100 ppm), Bromocresol green dye (100 ppm) and Bromophenol blue dye (100 ppm) respectively, the mixture was stirred for 60 min at $30 \text{ }^\circ\text{C}$, $40 \text{ }^\circ\text{C}$, $50 \text{ }^\circ\text{C}$, $60 \text{ }^\circ\text{C}$ and $70 \text{ }^\circ\text{C}$ respectively. The adsorption capacity was determined by the residual concentration of dye derived from absorbance and standard curve.

The adsorption kinetics was ascertained by Pseudo-first-order model and Pseudo-second-order model. The data on Pseudo-first-order model were calculated from the following Equation (Zhao and Wang 2017):

$$\log(q_e - q_t) = \log q_e - k_1/2.303 * t \quad (6)$$

The data on Pseudo-second-order model were calculated from the following Equation (Zhao and Wang 2017):

$$t/q_t = 1/k_2 * q_e^2 + 1/q_e * t \quad (7)$$

where q_e (mg/g) was the equilibrium adsorption amount, q_t (mg/g) was the adsorption amount at a time, k_1 (min^{-1}) and k_2 (g/mg.min) represented the coefficients of models, and t (min) represented the time of adsorption.

The adsorption isotherm curve was ascertained by Langmuir model. The data on Langmuir model were calculated from the following Equation (Zhao and Wang 2017):

$$q_e = b * q_{\text{max}} * C_e / (1 + bC_e) \quad (8)$$

where C_e (mg/L) was the residual concentration of dye at equilibrium, q_{max} (mg/g) was the largest adsorption amount, q_e (mg/g) was the equilibrium adsorption amount, and b (L/mg) represented the constant of Langmuir model.

The data on thermodynamic analysis were calculated from the following Equations (Fan et al. 2008; Lima et al. 2019):

$$K_e^0 = (1000 * K_L * \text{molecular weight of adsorbate}) / [\text{adsorbate}]^\circ / \gamma \quad (9)$$

$$\ln(K_e^0) = -\Delta H^0 / RT + \Delta S^0 / R \quad (10)$$

$$\Delta G^0 = -RT \ln(K_e^0) \quad (11)$$

$$\Delta G^0 = \Delta H^0 - T\Delta S^0 \quad (12)$$

where K_c^0 was the dimensionless hermodynamic equilibrium constant, γ was the coefficient of activity (dimensionless), $[\text{Adsorbate}]^\circ$ (1 mol/L) was the standard concentration of the adsorbate, K_L was the Langmuir equilibrium constant (given initially in L/mg converted into L/mol), the molecular weight of the adsorbate HPP2 (g/mol) was 39,892, R (8.314 J/mol.K) was the universal gas constant, ΔH^0 (KJ/mol) was the changes of enthalpy, ΔS^0 (KJ/mol.K) was the changes in the entropy, and ΔG^0 (KJ/mol) was the changes in Gibb's free energy.

The adsorption diffusion mode was ascertained by Intraparticle diffusion model and Membrane diffusion model. The data on Intraparticle diffusion model were calculated from the following Equation (Zhao and Wang 2017):

$$q_t = k_p * t^{1/2} + C \quad (13)$$

The data on Membrane diffusion model were calculated from the following Equations (Zhao and Wang 2017):

$$\ln(1 - F) = -k_f * t \quad (14)$$

$$F = q_t/q_e \quad (15)$$

where q_t (mg/g) was the adsorption amount at a time, q_e (mg/g) was the equilibrium adsorption amount, k_p (g/mg.min) and k_f (cm/s) represented the coefficients of models, C represented the constant of Intraparticle diffusion model, and t (min) represented the time of adsorption.

Results and discussion

DS of the modified hyperbranched hemicellulose polymer

The changes of DS on HCMA polymer and the modified hyperbranched hemicellulose polymer were described in Fig. 1. The DS of HCMA could reach the maximum 0.97, while the maximum DS of HPP1 was 0.89 and the maximum DS of HPP2 was 0.83. Introducing DMPA constantly, more active hydroxyl and carboxyl groups increased the branching degree of main chain. However, the growth of molecular chain and steric effect influenced the increase of DS on the modified hyperbranched hemicellulose polymer.

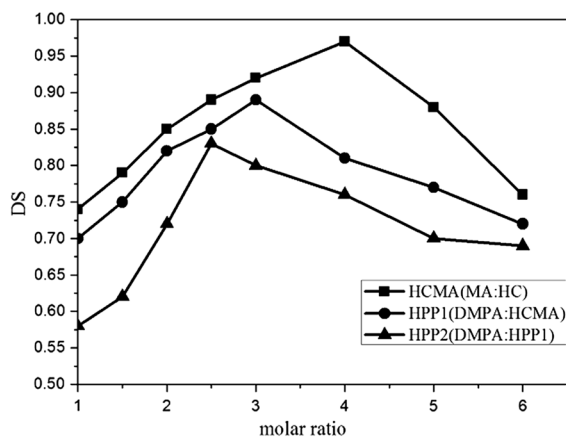


Fig. 1 The DS of the modified hyperbranched hemicellulose polymer

Additionally, more DMPA could cause the breakdown of the glycosylated bonds between hemicellulose groups, and reduce the increase of DS gradually. The prepared HPP2 with maximum DS was selected as adsorbent. The HPP2 with higher DS had more carboxyl groups and hydroxyl groups, which the dipole bond force and hydrogen bond force between the adsorbent HPP2 and the acid dye were stronger and the adsorption effect was better.

Kinematic viscosity of the modified hyperbranched hemicellulose polymer

The kinematic viscosity of HCMA polymer and the modified hyperbranched hemicellulose polymer were shown in Table 1. After HCMA polymer was grafted by DMPA, the long branched chain caused the increase of viscosity. With the increase of carboxyl and hydroxyl groups, the polarity and intermolecular force of the modified hyperbranched hemicellulose polymer were improved. The higher viscosity of the modified hyperbranched hemicellulose polymer was appropriate for absorbing dyes.

Structure analysis

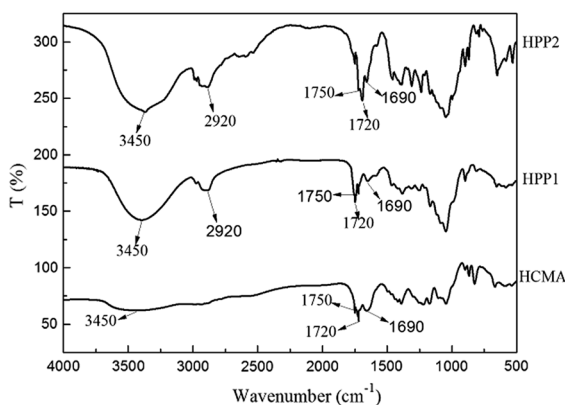
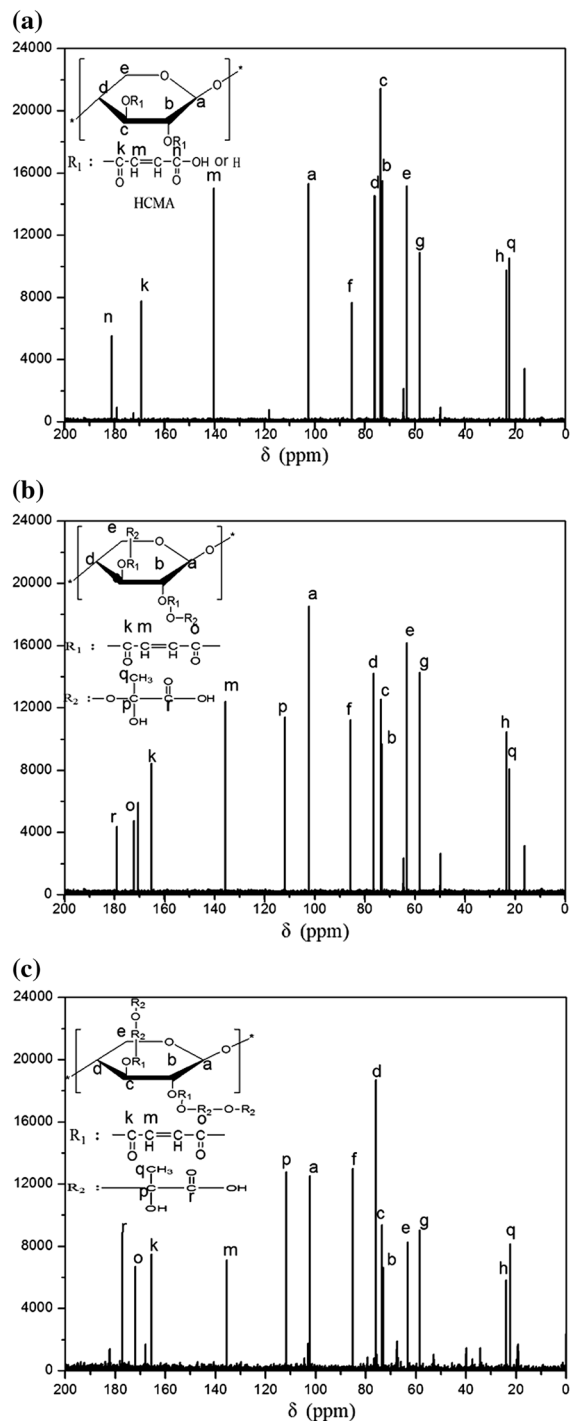
The FT-IR spectra of HCMA polymer and the modified hyperbranched hemicellulose polymer were shown in Fig. 2. The characteristic peaks of HCMA were at 3450 cm^{-1} ($-\text{OH}$), 1750 cm^{-1} ($-\text{COO}$), 1720 cm^{-1} ($-\text{COOH}$) and 1690 cm^{-1} ($-\text{C} = \text{C}-$)

Table 1 The kinematic viscosity of the modified hyperbranched hemicellulose polymer

Sample (g/ml)	Γ_r	Γ_s	Γ
Blank sample	1	0	0
HCMA	1.058	0.058	5.883
HPP1	1.084	0.084	8.741
HPP2	1.181	0.181	17.02

[indicated with HCMA in Fig. 2]. The characteristic peaks of HPP were at 3450 cm^{-1} ($-\text{OH}$), 2920 cm^{-1} ($-\text{CH}_3$), 1750 cm^{-1} ($-\text{COO}-$), 1720 cm^{-1} ($-\text{COOH}$), 1690 cm^{-1} ($-\text{C}=\text{C}-$) [indicated with HPP1 and HPP2 in Fig. 2]. Compared to the HCMA, the sample of HPP with more hydroxyl groups indicated a wide hydroxyl peak at 3450 cm^{-1} . When the DMPA with methyl group was grafted onto HCMA, the sample of HPP appeared the methyl peak at 2920 cm^{-1} . The sample of HPP2 with more carboxyl, hydroxyl and ester groups exhibited higher hydroxyl peak at 3450 cm^{-1} , ester peak at 1750 cm^{-1} and carboxyl peak at 1720 cm^{-1} than HPP1.

The ^{13}C -NMR spectra of HCMA polymer and the modified hyperbranched hemicellulose polymer were shown in Fig. 3a–c. The sample of HCMA showed characteristic peaks of carbon connected to double bond at 140.5 ppm , ester carbon at 169 ppm and carboxyl carbon at 181 ppm (Fig. 3a). With the introduction of DMPA, the spectrum of HPP increased the characteristic peaks of carboxyl carbon at 178 ppm , ester carbon at 172 ppm and hydroxyl

**Fig. 2** The FT-IR spectra of the modified hyperbranched hemicellulose polymer**Fig. 3** a The ^{13}C -NMR spectrum of the HCMA, b the ^{13}C -NMR spectrum of the HPP1 and c the ^{13}C -NMR spectrum of the HPP2

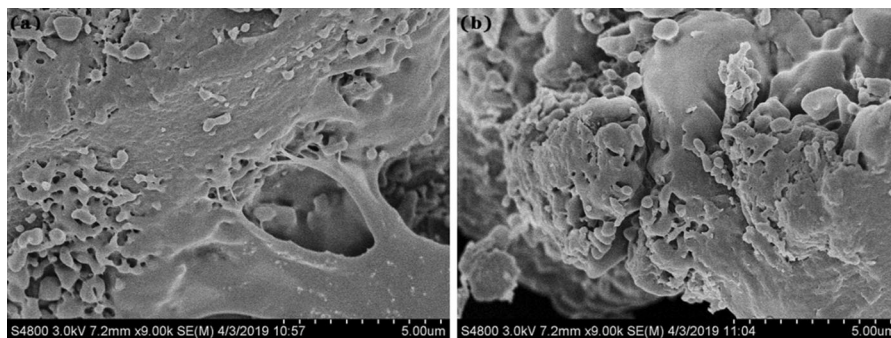


Fig. 4 **a** The SEM images of the HPP1 and **b** the SEM images of the HPP2

carbon at 112.3 ppm. Compared to the HPP1 (Fig. 3b), the sample of HPP2 showed higher strong peaks of terminal carboxyl carbon at 178 ppm, ester carbon at 172 ppm, hydroxyl carbon at 112.3 ppm and methyl carbon of the branched chain at 22.3 ppm, which could be attributed to more hydroxyl and carboxyl groups introduced from DMPA (Fig. 3c).

SEM analysis of the modified hyperbranched hemicellulose polymer

The SEM images of the hyperbranched hemicellulose HPP1 and HPP2 were shown in Fig. 4a, b. There were many pores in the surface of HPP1 and HPP2. With DMPA grafted gradually to the HPP2, more branched chains linked on the hemicellulose macromolecular. The HPP2 exhibited more distinct cross-linked structure than the HPP1. The pores and cross-linked structure were help for dye adsorption. When the hyperbranched hemicellulose polymer was used for dye adsorption, dye molecules could quickly cross the surface of macromolecules and adsorbed by the hyperbranched hemicellulose polymer. The pores and cross-linked structure increased the adsorption area and improved the adsorption capacity. Its structure showed a good prospect on adsorption application.

Thermal stability of the modified hyperbranched hemicellulose polymer

The Fig. 5 displayed the TGA and DTG curves of HCMA and the modified hyperbranched hemicellulose polymer HPP. All samples showed good thermal stability, and the temperature data were reported in

Table 2. The cross-linked network structure produced thermal stability at low temperature. As the branched ester chains were added on the linear units, the onset decomposition temperature of hyperbranched hemicellulose polymer was later than the HCMA polymer. The sample of HPP2 was grafted more branched ester chains, which resulted in the higher thermal stability. Because of the consistency of glycosidic bond fractured in hemicellulose molecular chain, the sample of HCMA, HPP1 and HPP2 exhibited the similar thermal decomposition curve (Fig. 5b). They had a strong degradation at about 268–278 °C, and the final degradation temperature was at about 568–596 °C (Table 2).

The adsorption capacity on HPP2 adsorbing acid dyes

The sample of HPP2 was applied in adsorbing Methyl red dye, Bromocresol green dye and Bromophenol blue dye. The influences on different dosage of HPP2, temperature and pH for adsorption capacity were shown in Fig. 6a–c. The dosage of HPP2 and temperature expressed the similar influence for three acid dyes, which the adsorption capacity began to increase quickly and then leveled off. When adding 4% HPP2, the adsorption capacity reached the maximum value (Fig. 6a). The optimum temperature was about 60 °C at which the adsorption capacity of Methyl red dye showed stronger (Fig. 6b). The pH had some different influences for adsorption capacity of three acid dyes. For the Bromocresol green dye and Bromophenol blue dye, the adsorption capacity increased with the rise of pH (Fig. 6c). While for Methyl red dye, the adsorption capacity decreased with the rise of pH. The pH could

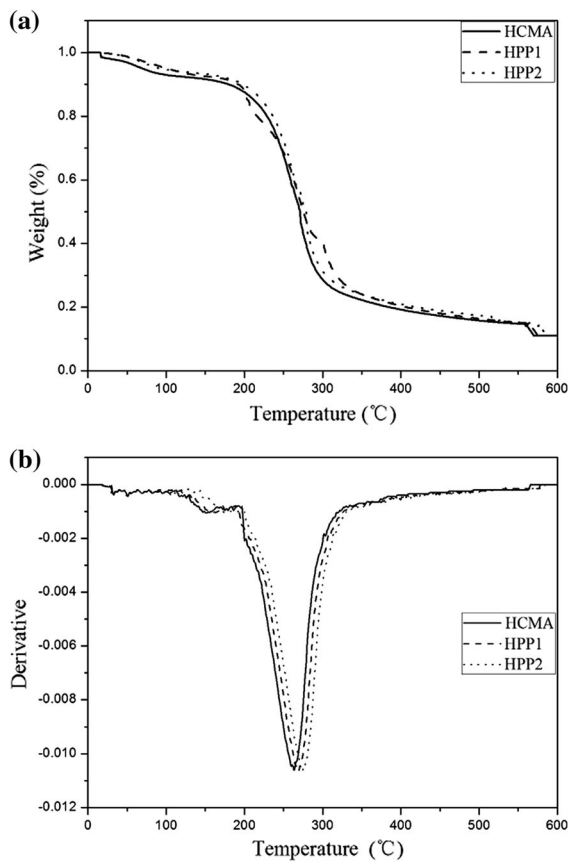


Fig. 5 **a** TGA curves of modified hyperbranched hemicellulose polymer and **b** DTG curves of modified hyperbranched hemicellulose polymer

Table 2 TGA data of the modified hyperbranched hemicellulose polymer

Sample	T10% (°C)	T50% (°C)	T90% (°C)
HCMA	179	268	571
HPP1	192	272	576
HPP2	197	278	587

not only affect the surface polarity of adsorbent and dye, but also affect the dissociation degree of terminal functional groups on adsorbent (Jayakumar et al. 2013; Zuo et al. 2011). As the pH increased, the carboxyl groups deprotonated gradually. Different functional groups on Methyl red, Bromocresol green and Bromophenol blue resulted unlike dipole bonding and H bonding forces on hyperbranched hemicellulose

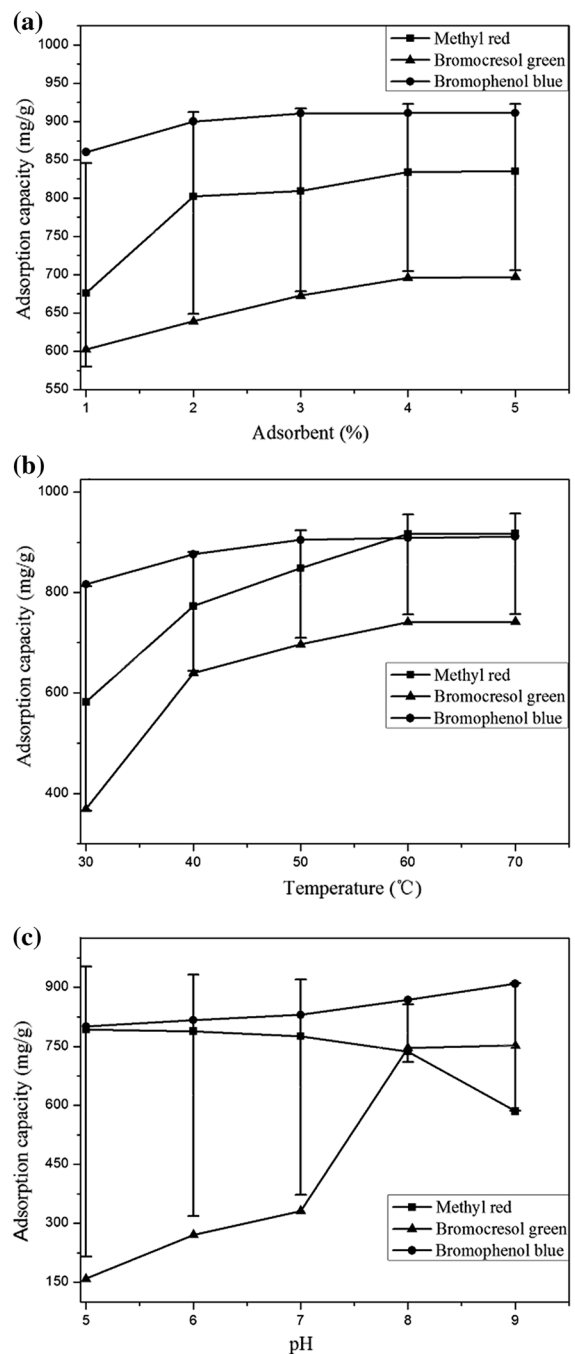


Fig. 6 **a** The adsorption capacity on different dosage of HPP2, **b** the adsorption capacity on different temperature and **c** the adsorption capacity on different pH

polymer. The adsorption capacity was affected by the change of adsorption force. The dipole bonding force

Fig. 7 **a** The adsorption capacity on different Ca^{2+} concentration, **b** the adsorption capacity on different Mg^{2+} concentration, **c** the adsorption capacity on different NO_3^- concentration and **d** the adsorption capacity on different SO_4^{2-} concentration

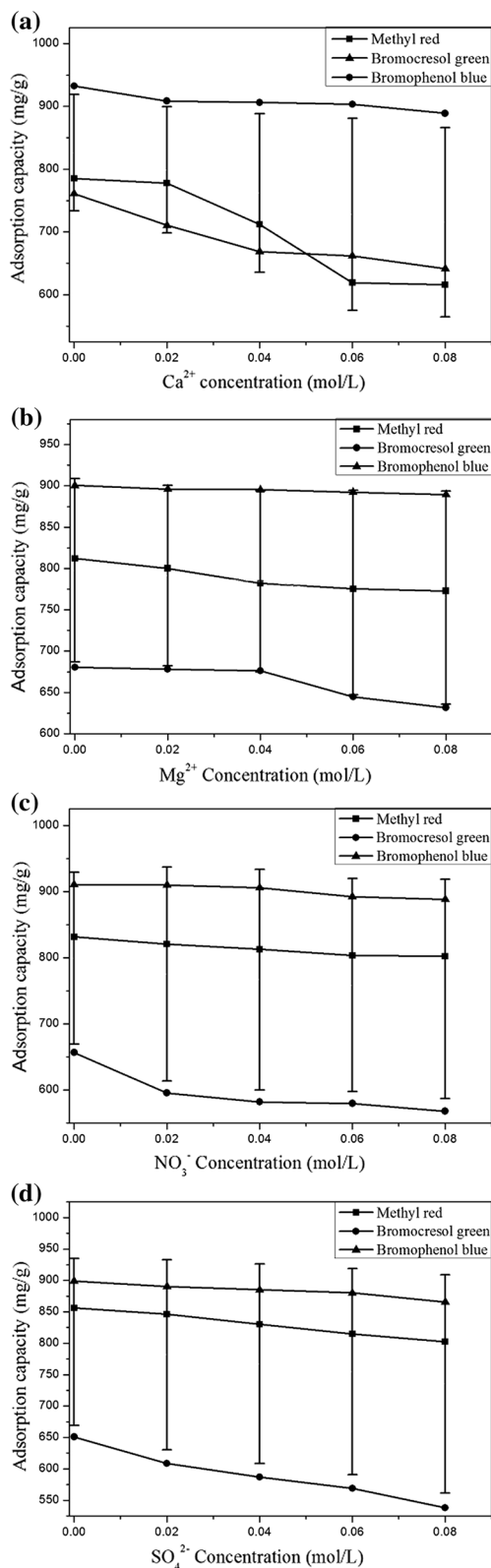
between HPP2 and Bromocresol green dye or Bromophenol blue dye were strengthened, and the adsorption capacity was improved. But for Methyl red dye, its carboxyl group increased the repulsion between HPP2 and dye, which led to the adsorption capacity reduce.

It could be seen that the dissociation degree of functional groups on Bromocresol green was more affected by the external environment than that of Methyl red and Bromophenol blue, resulting in a weak force between the adsorbent and Bromocresol green and a low adsorption capacity. The optimal adsorption capacity for Methyl red dye, Bromocresol green dye and Bromophenol blue dye could reach 825 mg/g, 675 mg/g and 912 mg/g respectively.

The changes of adsorption capacity caused by different ion strength were shown in Fig. 7a–d. The adsorption capacity at different concentration of Ca^{2+} , Mg^{2+} , NO_3^- and SO_4^{2-} showed the similar changes, which the adsorption capacity declined gradually as the increase of concentrations of ion strength. The results revealed that the existence of charged ion would cause the competitive adsorption among hyperbranched hemicellulose polymer, dye and charged ion, which resulted in some negative influence for adsorption between hyperbranched hemicellulose polymer and dyes.

The adsorption mechanism analysis on HPP2 adsorbing acid dyes

The kinetic adsorption curves on HPP2 adsorbing three dyes were shown in Figs. 8a–c and 9a–c, and the related kinetic adsorption data were listed in Table 3. The kinetic adsorption curves could be explained by the related kinetic adsorption data. For Methyl red dye as example, the R^2 of the Pseudo-first-order kinetics adsorption data were 0.899, 0.759 and 0.634 respectively. While the R^2 of the Pseudo-second-order kinetics adsorption data were 0.995, 0.998 and 0.996 respectively. Obviously, the Pseudo-second-order kinetics model showed better consistency than the Pseudo-first-order kinetics model according to the correlation coefficient of R^2 close to 1. Moreover, the data of q_e obtained by matching the Pseudo-second-



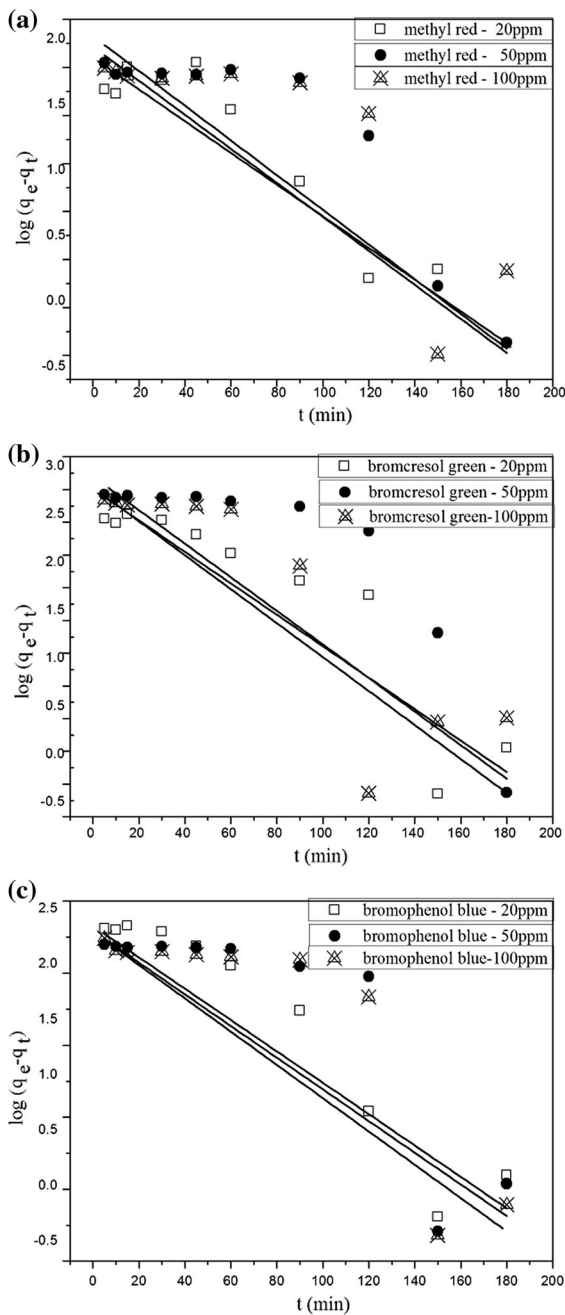


Fig. 8 **a** The pseudo-first-order kinetic adsorption curves on HPP2 adsorbing methyl red dye, **b** the pseudo-first-order kinetic adsorption curves on HPP2 adsorbing Bromocresol green dye and **c** the pseudo-first-order kinetic adsorption curves on HPP2 adsorbing Bromophenol blue dye

order kinetic adsorption curve were 28.56 mg/g, 113.6 mg/g and 234.9 mg/g respectively, which were close to the data obtained from the experiment. The

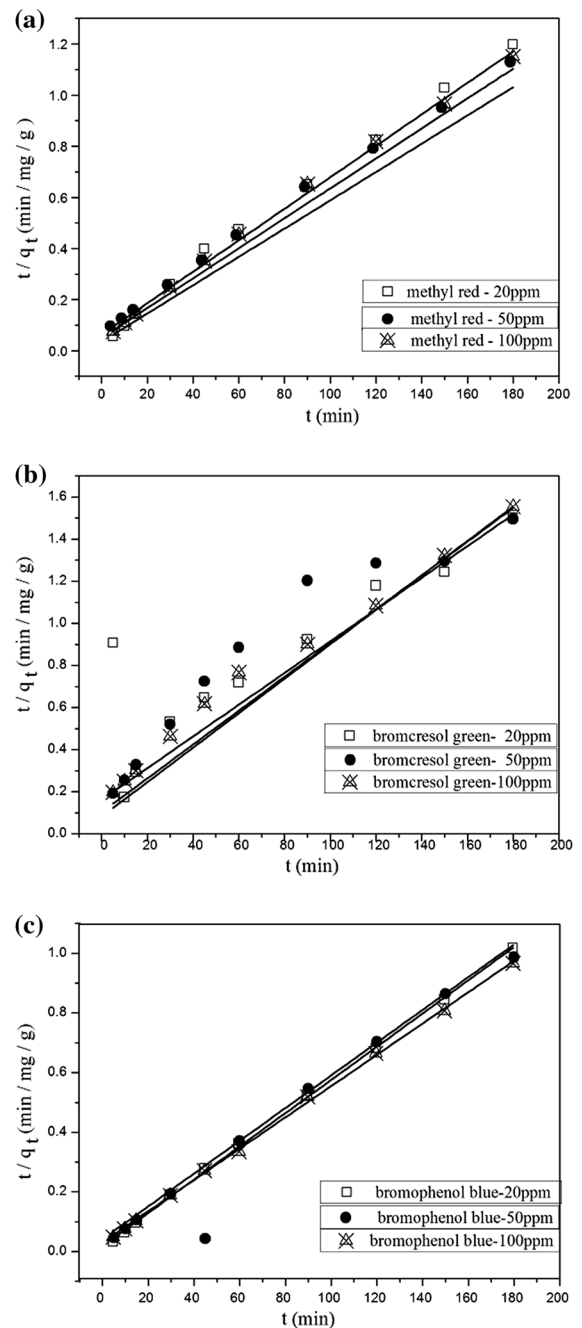


Fig. 9 **a** The pseudo-second-order kinetic adsorption curves on HPP2 adsorbing methyl red dye, **b** the pseudo-second-order kinetic adsorption curves on HPP2 adsorbing bromocresol green dye and **c** the pseudo-second-order kinetic adsorption curves on HPP2 adsorbing bromophenol blue dye

data of HPP2 adsorbing Bromocresol green dye and Bromophenol blue dye were also met with the Pseudo-second-order kinetics model well.

Table 3 The kinetic adsorption data on HPP2 adsorbing dyes

Sample	C ₀ (ppm)	Pseudo-first-order kinetic adsorption date			Pseudo-second-order kinetic adsorption date		
		k ₁ (× 10 ⁻¹) (min ⁻¹)	q _e (mg/g)	R ²	k ₂ (× 10 ⁻²) (g/mg min)	q _e (mg/g)	R ²
Methyl red dye	20	7.32	0.981	0.899	22.1	28.56	0.995
	50	8.49	0.973	0.759	3.40	113.6	0.998
	100	10.3	0.972	0.634	1.60	234.9	0.996
Bromcresol green dye	20	8.95	0.976	0.807	511	5.091	0.997
	50	11.6	0.973	0.662	142	15.03	0.991
	100	11.7	0.963	0.767	13.4	75.19	0.987
Bromophenol blue dye	20	6.67	0.973	0.905	4.60	62.33	0.999
	50	8.69	0.971	0.658	1.40	175.8	0.997
	100	9.77	0.966	0.699	26.5	58.52	0.999

The adsorption isotherm analysis on HPP2 adsorbing acid dyes

The adsorption isotherms curves on HPP2 adsorbing three dyes based on Langmuir model were shown in Fig. 10a–c, and the related adsorption isotherm data were listed in Table 4. The adsorption capacity was improved with the increase of temperature and then gradually stabilized (Fig. 10a–c). The adsorption isotherms curves could be explained by the related adsorption isotherm data. For HPP2 adsorbing Methyl red dye as example, the data of R² were 0.962, 0.981 and 0.982 at 30 °C, 40 °C and 50 °C respectively. The date of R² closing to 1 suggested that the adsorption could well consistent with Langmuir isothermal adsorption model (Table 4). The data of q_{max} were 287.5 mg/g, 289.9 mg/g and 301.2 mg/g respectively, and their slight change with the increase of temperature indicated that the process of adsorption was endothermic. The data of K_L were changed from 3.521*10⁻² L/mg, 3.940*10⁻² L/mg to 3.978*10⁻² L/mg at 30 °C, 40 °C and 50 °C respectively, which implied that raising temperature could strengthen the HPP2 adsorbing Methyl red dye. According to the same analysis, the process of HPP2 adsorbing Bromcresol green dye and Bromophenol blue dye also met with Langmuir isothermal adsorption model. Above results revealed that the adsorption process of HPP2 on acid dyes was monolayer adsorption. At the same time, it may include physical adsorption process and electrostatic attraction process.

The thermodynamic analysis on HPP2 adsorbing acid dyes

Thermodynamic data on HPP2 adsorbing three dyes were listed in Tables 5 and 6. For HPP2 adsorbing Methyl red dye as example, the data of ΔG⁰ were – 35.65 kJ/mol, – 37.11 kJ/mol and – 38.23 kJ/mol respectively under 303 K, 313 K and 323 K. The negative ΔG⁰ indicated that the adsorption process was spontaneous. With the increase of temperature, the functional groups on adsorbent surface possessed more active energy. The temperature affected the thickness of the boundary layer around the adsorbent, which could change the diffusion rate of dyes (Tian et al. 2010). The variation of ΔG⁰ met the physical adsorption process, which was consistent with the results of adsorption isotherms analysis. The negative ΔH⁰ indicated the endothermic adsorption process, and increasing temperature would conducive to the adsorption. The date of ΔS⁰ was 72.65 kJ/mol.K, 72.85 kJ/mol.K and 73.11 kJ/mol.K respectively, which suggested a certain degree of chaotic on solid–liquid interface. The thermodynamic data testified HPP2 had a strong adsorption capacity for acid dyes.

The N₂-adsorption/desorption isotherms analysis on HPP2

The N₂-adsorption/desorption isotherms of HPP2 were shown in Fig. 11. Above was the adsorption curve and below was the desorption curve. At the low

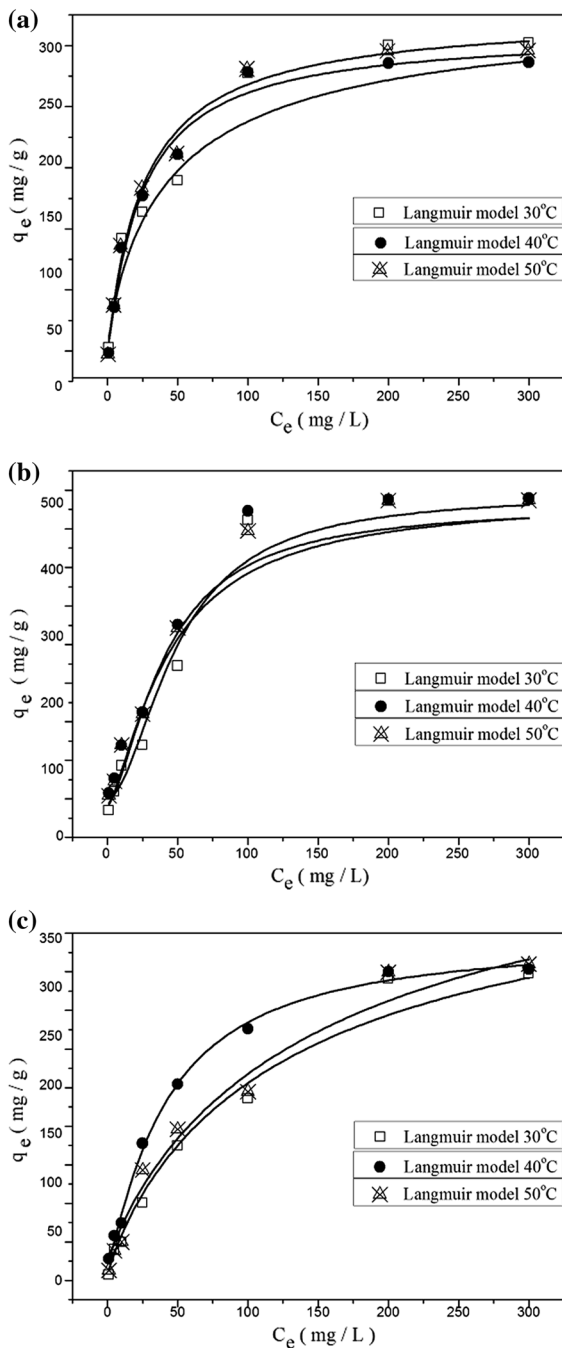


Fig. 10 **a** Langmuir adsorption isotherm curves on HPP2 adsorbing methyl red dye, **b** Langmuir adsorption isotherm curves on HPP2 adsorbing Bromocresol green dye and **c** Langmuir adsorption isotherm curves on HPP2 adsorbing Bromophenol blue dye

relative pressure, the interaction between HPP2 and N_2 was weak resulted the slow increase of amount adsorbed. When the relative pressure was 0.12, the desorption rate was only 35.1% (which was the ratio of desorption amount and adsorption amount). Then the relative pressure was improved, the amount adsorbed increased rapidly. When the relative pressure was above 0.82, the desorption rate exceeded 80%. At the higher relative pressure, the HPP2 could be successfully regenerated and repeatedly used in N_2 adsorption. The N_2 -adsorption/desorption isotherms revealed that the modified hyperbranched hemicellulose polymer filled the pore in clusters, and its adsorption process met with monolayer adsorption. The analysis of N_2 -adsorption/desorption isotherms was consistent with the results of adsorption isotherms and thermodynamic analysis.

The diffusion mode analysis on HPP2 adsorbing acid dyes

Generally, the study on diffusion followed the theory of four-step adsorption process. First, the dye moved to the liquid film surface of the adsorbent, which was called Bulk diffusion. Secondly, the dye moved toward the surface of the adsorbent and passed through the liquid film surface of the adsorbent, which was called Membrane diffusion. Thirdly, the dye continued to move into the inside of adsorbent, which was called Interparticle diffusion. Fourthly, the dye was adsorbed by physical or physicochemical processes, which was the Solute sorption. Also, many researches had shown that the first and fourth steps did not generally become rate control steps, and the second and third step were the most likely control steps (Ozcan 2005; Karthik and Meenakshi 2015). It was necessary to build the diffusion curves based on Intraparticle diffusion model and Membrane diffusion model to ascertain the diffusion theory of HPP2 in adsorption process.

The diffusion curves on HPP2 adsorbing three acid dyes based on Intraparticle diffusion model and Membrane diffusion model were shown in Figs. 12a–c and 13a–c, and the related diffusion data were listed in Table 7. The diffusion rate varied with the initial concentration of dye (Figs. 12a–c, 13a–c). The adsorption diffusion theory on HPP2 adsorbing three acid dyes could be discovered by the related diffusion data. For HPP2 adsorbing Bromophenol blue

Table 4 The Langmuir adsorption isotherm data on HPP2 adsorbing dyes

Sample	Temperature (°C)	Langmuir adsorption isotherm data		
		q_{\max} (mg/g)	$K_L(\times 10^{-2})$ (L/mg)	R^2
Methyl red dye	30	287.5	3.521	0.962
	40	289.9	3.940	0.981
	50	301.2	3.978	0.982
Bromocresol green dye	30	395.2	0.034	0.967
	40	448.9	0.370	0.976
	50	507.4	0.570	0.984
Bromophenol blue dye	30	261.2	1.081	0.982
	40	282.7	1.105	0.996
	50	456.6	1.138	0.978

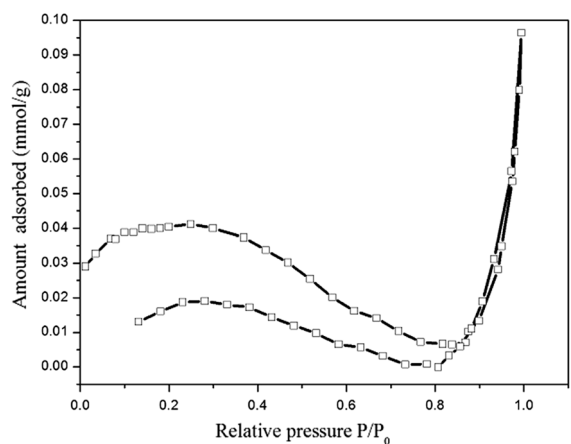
Table 5 Equilibrium constants based on Eq. (9)

Sample	K_L (L/mg)			K_L (L/mol)			K_e^0			$\ln K_e^0$		
	303 K	313 K	323 K	303 K	313 K	323 K	303 K	313 K	323 K	303 K	313 K	323 K
Methyl red dye	-13.64	-14.31	-14.62	72.65	72.85	73.11	-35.65	-37.11	-38.23	14.15	14.26	14.27
Bromocresol green dye	-9.252	-10.47	-11.69	48.54	65.48	66.35	-23.96	-30.97	-33.72	9.510	11.90	12.33
Bromophenol blue dye	-12.05	-12.28	-12.38	67.79	68.95	70.01	-32.62	-33.86	-34.99	12.95	13.01	13.03

Table 6 Thermodynamic data on HPP2 adsorbing dyes

Sample	ΔH^0 (KJ/mol)			ΔS^0 (KJ/mol.K)			ΔG^0 (KJ/mol)		
	303 K	313 K	323 K	303 K	313 K	323 K	303 K	313 K	323 K
Methyl red dye	-13.64	-14.31	-14.62	72.65	72.85	73.11	-35.65	-37.11	-38.23
Bromocresol green dye	-9.252	-10.47	-11.69	48.54	65.48	66.35	-23.96	-30.97	-33.72
Bromophenol blue dye	-12.05	-12.28	-12.38	67.79	68.95	70.01	-32.62	-33.86	-34.99

dye as example, the R^2 of Intraparticle diffusion model were 0.942, 0.760 and 0.806 at 20 ppm, 50 ppm and 100 ppm respectively, while the R^2 of Membrane diffusion model were 0.904, 0.427 and 0.484 at 20 ppm, 50 ppm and 100 ppm respectively. Obviously the adsorption was more conformed to the Intraparticle diffusion model. Moreover, it could be discovered that the intercepts of both diffusion model were not 0 (Table 7), which indicated the adsorption was not controlled by one model but by both models simultaneously. The diffusion modes obtained by HPP2 adsorbing Methyl red dye, Bromocresol green dye and Bromophenol blue dye were consistent with the adsorption diffusion theory of which the adsorption rate was controlled both by Intraparticle diffusion

**Fig. 11** The N_2 -adsorption/desorption isotherms of HPP2

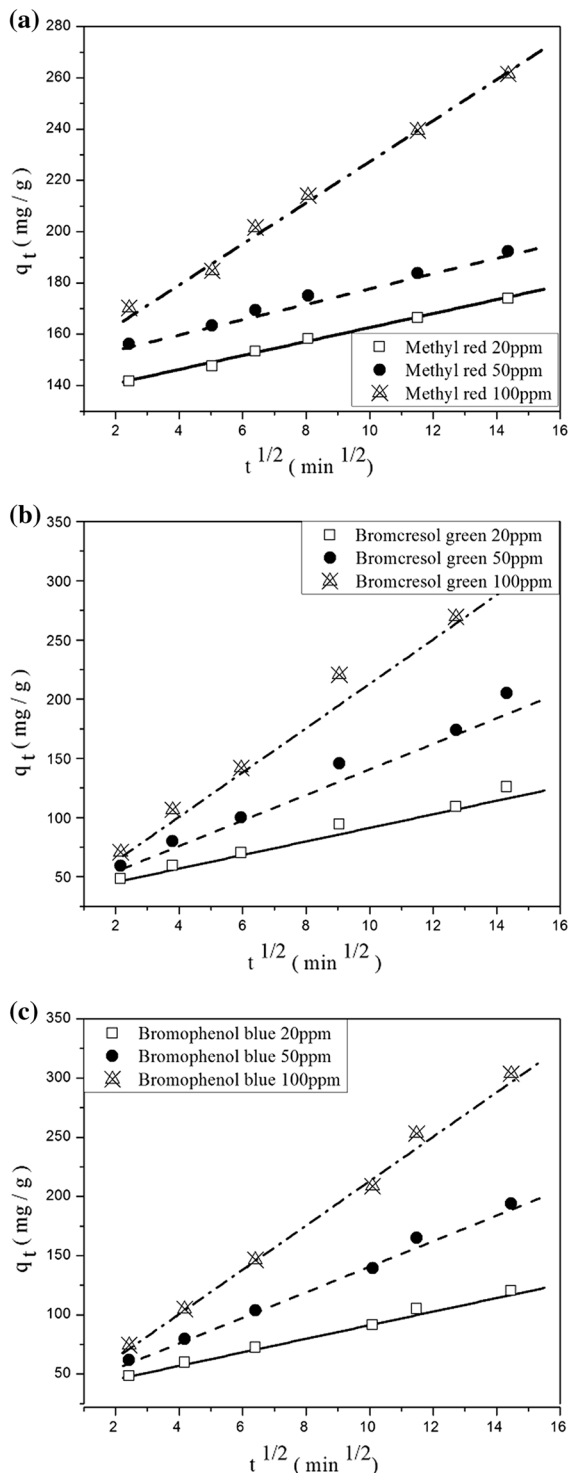


Fig. 12 **a** The intraparticle diffusion curves of HPP2 adsorbing methyl red dye, **b** the intraparticle diffusion curves of HPP2 adsorbing bromocresol green dye and **c** the intraparticle diffusion curves of HPP2 adsorbing bromophenol blue dye

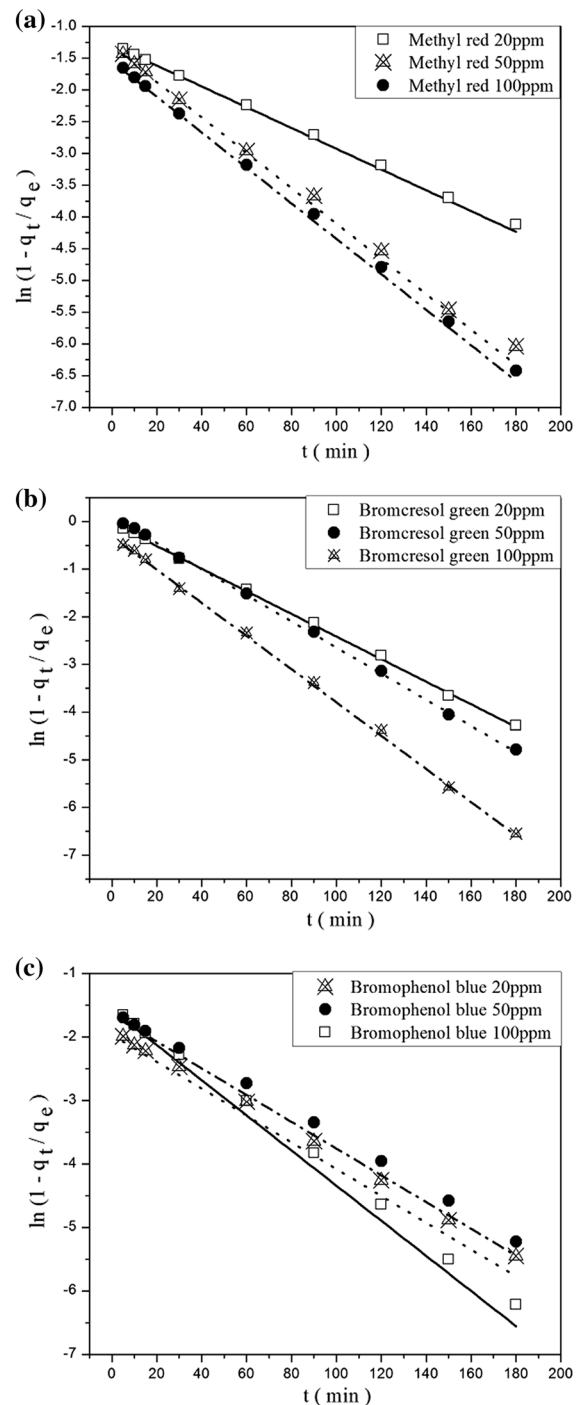


Fig. 13 **a** The membrane diffusion curves of HPP2 adsorbing methyl red dye, **b** the membrane diffusion curves of HPP2 adsorbing bromocresol green dye and **c** the membrane diffusion curves of HPP2 adsorbing bromophenol blue dye

Table 7 The diffusion data of HPP2 adsorbing dyes

Sample	C ₀ (ppm)	Intraparticle diffusion date			Membrane diffusion date		
		K _p (g/mg min)	Intercept	R ²	K _f (× 10 ⁻²) (cm/s)	Intercept	R ²
Methyl red dye	20	2.723	135.4	0.866	16	– 1.290	0.902
	50	2.997	377.7	0.698	28	– 1.550	0.761
	100	8.016	767.2	0.721	29	– 1.720	0.738
Bromocresol green dye	20	5.731	33.89	0.944	24	– 0.041	0.808
	50	10.08	127.7	0.746	28	– 0.095	0.676
	100	18.74	444.6	0.831	42	– 0.279	0.725
Bromophenol blue dye	20	1.909	144.9	0.942	28	– 1.574	0.904
	50	3.091	391.7	0.760	21	– 1.651	0.427
	100	5.164	828.4	0.806	21	– 1.967	0.484

model and Membrane diffusion model, and Intraparticle diffusion model affected more.

Conclusions

The modified hyperbranched hemicellulose polymer (HHP) was synthesized and analyzed by degree of substitution, kinematic viscosity, FT-IR, ¹³C-NMR, TGA and SEM. The modified hyperbranched hemicellulose polymer had high branched degree and possessed a large number of terminal carboxyl groups and hydroxyl groups. In SEM images, the HHP exhibited the pores and cross-linked structure which were good help for dye adsorption. The adsorption capacity on HPP2 adsorbing ethyl red dye, Bromocresol green dye and Bromophenol blue dye were studied through the adsorbent dosage, pH, temperature and ionic strength. The adsorption capacity was influenced significantly by different adsorbent dosage, pH, temperature and ionic strength. The adsorption mechanism of HPP2 adsorbing three acid dyes were accordance with the Pseudo-second-order kinetic model better. The adsorption isotherms were more matched with Langmuir model, and the data indicated that raising temperature could improve the adsorption capacity. The results of adsorption isotherms and thermodynamic data all indicated the processes of HPP2 adsorbing three acid dyes were endothermic. The N₂-adsorption/desorption isotherms of HPP2 revealed the hyperbranched hemicellulose polymer filled the pore in clusters, and its adsorption process

met with monolayer adsorption. The adsorption diffusion mode on HPP2 adsorbing three acid dyes were discussed by Intraparticle diffusion model and Membrane diffusion model. The adsorption rate was controlled both by Intraparticle diffusion model and Membrane diffusion model, of which Intraparticle diffusion model affected more. The optimal adsorption capacity of HPP2 on Methyl red, Bromomethyl green and Bromophenol blue could reach 825 mg/g, 675 mg/g and 912 mg/g respectively, which were better than many macromolecules for adsorbing organic dyes. Compared with others' research works, the HHP have a variety of active groups, and as a new, non-pollution adsorbent it exhibits high efficiency and adaptability in dye adsorption. At the same time, the HHP can well meet the needs of regeneration and reuse.

Acknowledgments Valuable cooperation of Prof. Hanjiang Yu from Tangshan Sanyou Group Xingda Chemical Fibre Co. Ltd. is greatly appreciated by the authors.

Funding This study was funded by Bureau of Science and Technology of Hebei Province (16211223D).

Compliance with ethical standards

Conflict of interest The authors declare that they have no conflict of interest.

References

Bodnar M, Kjoniksen A, Molnar R, Hartmann J, Daroczi L, Nystrom B, Borbely JY (2007) Nanoparticles formed by

- complexation of poly- γ -glutamic acid with lead ions. *J Hazard Mater* 153:1185–1192. <https://doi.org/10.1016/j.jhazmat.2007.09.080>
- Chen Z, Zhou L, Zhang F, Yu C, Wei Z (2012) Multicarboxylic hyperbranched polyglycerol modified SBA-15 for the adsorption of cationic dyes and copper ions from aqueous media. *J Appl Surf Sci* 258:5291–5298. <https://doi.org/10.1016/j.apsusc.2012.02.021>
- Esposito D, Antonietti M (2015) Redefining biorefinery: the search for unconventional building blocks for materials. *J Chem Soc Rev* 44:5821–5835. <https://doi.org/10.1039/c4cs00368c>
- Fan T, Liu YG, Feng BY, Zeng GM, Yang CP, Zhou M, Zhou HZ, Tan ZF, Wang X (2008) Biosorption of cadmium(II), zinc(II) and lead(II) by *penicillium simplicissimum*: isotherms, kinetics and thermodynamics. *J Hazard Mater* 160:655–661. <https://doi.org/10.1016/j.jhazmat.2008.03.038>
- Fan W, Gao W, Zhang C, Tjium WW, Pan J, Liu T (2012) Hybridization of graphene sheets and carbon-coated Fe_3O_4 nanoparticles as a synergistic adsorbent of organic dyes. *J Mater Chem* 22:25108–25116. <https://doi.org/10.1039/c2jm35609k>
- Ferrari E, Ranucci E, Edlund U, Albertsson AC (2015) Design of renewable poly (amidoamine)/hemicellulose hydrogels for heavy metal adsorption. *J App Polym Sci* 132: 41682–41695. <https://doi.org/10.1002/app.41695>
- Guijarro-Aldaco A, Hernandez-Montoya V, Bonilla-Petriciolet A, Montes-Moran MA, Mendoza-Castillo DI (2011) Improving the adsorption of heavy metals from water using commercial carbons modified with egg shell wastes. *J Chem Eng* 50:9354–9362. <https://doi.org/10.1021/ie2006627>
- Hu QK (2008) Preparation of modified chitosan and discoloration of dyeing and printing wastewater. *Text Auxiliaries* 25:253–256. <https://doi.org/10.3969/j.issn.1004-0439.2008.03.005>
- Hu XJ, Wang JS, Liu YG et al (2011) Adsorption of chromium (VI) by ethylenediamine-modified cross-linked magnetic chitosan resin: isotherms, kinetics and thermodynamics. *J Hazard Mater* 185:306–314. <https://doi.org/10.1016/j.jhazmat.2010.09.034>
- Jayakumar S, Gomathi T, Sudha PN (2013) Sorption studies of lead (II) onto crosslinked and non crosslinked biopolymeric blends. *J Biol Macro* 59:165–169. <https://doi.org/10.1016/j.jbiomac.2013.04.031>
- Kanekiyo Y, Tao H, Sellergren B (2008) Stimuli-responsive guest binding and releasing by dendritic polymer-based hydrogels. *J Polymer* 40:684–687. <https://doi.org/10.1295/polymj.PJ2008018>
- Karthik R, Meenakshi S (2015) Removal of Pb(II) and Cd(II) ions from aqueous solution using polyaniline grafted chitosan. *J Chem Eng* 263:168–177. <https://doi.org/10.1016/j.cej.2014.11.015>
- Li B, Jiang X, Yin J (2012) Multi-responsive microgel of hyperbranched poly(ether amine) (hPEA-mGel) for the selective adsorption and separation of hydrophilic fluoresce in dyes. *J Mater Chem* 22:17976–17983. <https://doi.org/10.1039/C2JM33188H>
- Lima EC, Hosseini-Bandegharai A, Moreno-Piraján JC, Anastopoulos I (2019) A critical review of the estimation of the thermodynamic parameters on adsorption equilibria. *J Mol Liq* 273:425–434. <https://doi.org/10.1016/j.molliq.2018.10.048>
- Lu L, Zhao H, Yan L, Wang G, Mao Y, Wang X, Jiang T (2015) Removal characteristics of Cd(II) ions from aqueous solution on ordered mesoporous carbon. *J Chem Eng* 32:2161–2167. <https://doi.org/10.1007/s11814-015-0150-7>
- Luo Y, Zhang C, Xu F, Chen Y, Fan L, Wei Q (2010) Synthesis and characterization of novel THTPBA/PEG-derived polyurethane scaffolds for tissue engineering. *J Mater Sci* 45:1866–1877. <https://doi.org/10.1007/s10853-009-4171-7>
- Moran JL, Cyrus VP, Vazquez A (2012) Preparation and characterization of three different derivatized potato starches. *J Polym Environ* 21:395–404. <https://doi.org/10.1007/s10924-012-0539-x>
- Ning L, Liao S, Sun Y, Yu L, Tong X (2016) The efficient oxidation of biomass-derived 5-hydroxymethyl furfural to produce 2,5-diformylfuran over supported cobalt catalysts. *J Chem Rev* 9:95–101. <https://doi.org/10.1007/s12649-016-9724-9>
- Ozcan A (2005) Adsorption of acid red 57 from aqueous solutions onto surfactant-modified sepiolite. *J Hazard Mater* 125:252–259. <https://doi.org/10.1016/j.jhazmat.2005.05.039>
- Peng Y, Wang KK, Liu T, Xu J, Xu BG (2017) Synthesis of one-dimensional Bi_2O_3 - Bi_2O_2 heterojunctions with high interface quality for enhanced visible light photocatalysis in degradation of high-concentration phenol and MO dyes. *J Appl Catal Environ* 203:946–954. <https://doi.org/10.1039/c8ce00101d>
- Ragauskas AJ (2006) The path forward for biofuels and biomaterials. *J Sci* 311:484–489. <https://doi.org/10.1126/science.1114736>
- Rahman ML, Sarkax SM, Yusoff MM et al (2017) Optical detection and efficient removal of transition metal ions from water using poly (hydroxamic acid) ligand. *J Sens Actuators B Chem* 242:595–608. <https://doi.org/10.1016/j.snb.2016.11.007>
- Schutyser W, Renders T, Vanden BS, Koelewijn SF (2018) Chemicals from lignin: an interplay of lignocellulose fractionation, depolymerisation and upgrading. *J Chem Soc Rev* 47:852–908. <https://doi.org/10.1039/C7CS00566K>
- Sun K, Shi Y, Xu W, Potter N, Li Z, Zhu J (2017) Modification of clays and zeolites by ionic liquids for the uptake of chloramphenicol from water. *J Chem Eng* 313:336–344. <https://doi.org/10.1016/j.cej.2016.12.083>
- Tian Y, Ji C, Zhao M (2010) Preparation and characterization of baker's yeast modified by nano- Fe_3O_4 : application of biosorption of methyl violet in aqueous solution. *J Chem Eng* 165:474–481. <https://doi.org/10.1016/j.cej.2010.09.037>
- Tirtom VN, Dincer A, Becerik S, Aydemir T, Celik A (2012) Comparative adsorption of Ni(II) and Cd(II) ions on epichlorohydrin crosslinked chitosan-clay composite beads in aqueous solutions. *J Environ Sci* 22:379–386. <https://doi.org/10.1016/j.cej.2012.05.059>
- Tripathi N, Choppala G, Singh RS, Srivastava P, Seshadri B (2016) Adsorption kinetics of zinc and nickel on modified chitosan. *J Hazard Mater* 188:507–520. <https://doi.org/10.1007/s10661-016-5499-5>

- Voit BI, Lederer A (2009) Hyperbranched and highly branched polymer architectures-synthetic strategies and major characterization aspects. *J Chem Rev* 109:5924–5973. <https://doi.org/10.1021/cr900068q>
- Wang J, Wang D, Zhang G, Guo Y, Liu J (2013) Adsorption of rhodamine B from aqueous solution onto heat-activated sepiolite. *J Hazard Mater* 18:219–225. <https://doi.org/10.1007/s11859-013-0918-8>
- Zhao S, Wang Z (2017) A loose nano-filtration membrane prepared by coating HPAN UF membrane with modified PEI for dye reuse and desalination. *J Membr Sci* 524:214–224. <https://doi.org/10.1016/j.apcatb.2016.11.011>
- Zheng Y, Li S, Weng Z, Gao C (2015) Hyperbranched polymers: advances from synthesis to applications chemical. *J Soc Rev* 44:4091–4130. <https://doi.org/10.1039/c4cs00528g>
- Zhou L, He B, Huang J (2013) One-step synthesis of robust amine- and vinyl-capped magnetic iron oxide nanoparticles for polymer grafting and in dye adsorption and catalysis. *J Appl Mater Interface* 5:8678–8685. <https://doi.org/10.1021/am402334f>
- Zhu W, Liu L, Liao Q, Chen X, Qian Z, Shen J, Liang J, Yao J (2016) Functionalization of cellulose with hyperbranched polyethylenimine for selective dye adsorption and separation. *J Cellul* 23:3785–3797. <https://doi.org/10.1007/s10570-016-1045-4>
- Zuo L, Yu S, Zhou H, Jiang J, Tian X (2011) Adsorption of Eu(III) from aqueous solution using mesoporous molecular sieve. *J Radioanal Nucl Chem* 288:579–586. <https://doi.org/10.1007/s10967-010-0972-z>

Publisher's Note Springer Nature remains neutral with regard to jurisdictional claims in published maps and institutional affiliations.